OMAE2021-63010

Numerical Investigation of an Experimental Ocean Current Turbine Based on Blade Element Momentum Theory (BEM)

S. Sadeqi	S. Rouhi
University of New	University of New
Orleans	Orleans
New Orleans, LA	New Orleans, LA
I Van Zwieten	C 6

N. Xiros University of New Orleans New Orleans, LA E. Aktosun University of New Orleans New Orleans, LA

J. VanZwieten
Florida Atlantic University
Boca Raton, FL

C. Sultan Virginia Tech. Blacksburg, VA J. loup University of New Orleans New Orleans, LA

ABSTRACT

Ocean currents are one of the alternative sources of green, sustainable, and renewable energy that could generate low-cost electric power without any pollution due to the burning of fossil fuels. Due to the density of the water, ocean currents can produce a significant amount of energy even with a very small current velocity field. In this study, a comprehensive performance analysis of 3-blade horizontal-axis Ocean Current Turbine (OCT) is shown to achieve optimal rpm (revolutions per minute) to match environmental conditions in order to harvest the maximum possible energy from OCT in ocean currents. Our approach is to use Blade Element Momentum (BEM) theory in order to estimate hydrodynamic loads for the turbine; specifically, the design of the OCT blades is based on a FX77-W121 type airfoil. We use JavaFoil to analyze and determine hydrodynamic lift and drag coefficients with respect different angles of attack for the hydrofoil profiles in seawater. After validation of blade design characteristics and obtaining the local coefficients of each hydrofoil cross-sections, we transfer them to our in-house-developed Blade Element Momentum Theory (BEM) code in order to achieve the estimation of performance analysis of the OCT in order to get maximum power and ideal torque and thrust. This performance analysis with BEM model of the OCT is an important step for further analysis due to having different incoming flow speeds in actual timevarying sea conditions. Indeed, the OCT will encounter different incoming ocean current speeds during operation. Therefore, this

approach is used to get an accurate brake power estimate of the OCT in different operational current speeds. In addition, this performance analysis of the OCT is going to be utilized in designing and developing a test model for the physical towing tank experiment for later investigation.

Keywords: Ocean Current, Sustainable, Green Energy, Renewable Energy, Electric Power, Current Velocity Field, Hydrokinetic Energy, Ocean Current Turbine (OCT), Horizontal Axis OCT, Blade Element Momentum (BEM) Theory, Lift Coefficient, Drag Coefficient, Performance Analysis, Power Estimation, OCT Design, Towing Tank Experiment.

NOMENCLATURE

A	Cross Sectional Area
ρ	Density of the Sea-water
U	Flow Velocity
a	Axial Flow Induction Factor
a'	Tangential Flow Induction Factor
Ω	Angular Velocity
r	Radius of the Actuator disc/ The Local Radius
the Rotor	
R	Rotor Radius

Resultant Velocity

on

W

cChord LengthNNumber of Blades β Set Pitch Angle α Angle of Attack (AOA) α Local Inflow Angle

 φ Local Inflow Angle C_l Lift Coefficient C_d Drag Coefficient

 δL Cross Sectional Lift Force δD Cross Sectional Drag Force

F Tip Loss Factor

Q Torque P Power T Thrust

1. INTRODUCTION

Hydrokinetic energy extraction has seen an increase in interest in response to growing demand of energy production from renewable resources. Especially, in the form of ocean current due to its continual availability and the capability of generating power without making a serious change to the surroundings. In addition to the high-power density of the ocean current in compare to other source of renewable energy, the predictable behavior of these currents makes it a reliable power generation substitute. We need to develop new and reliable technologies to harness ocean currents and extract the maximum hydrokinetic energy from the ocean and convert it into reliable and usable energy. Ocean current turbines (OCT) work on the same principle as wind turbines. Hence, an OCT has been designed and analyzed using numerical method. This numerical method was based on blade element momentum theory which modified by Prandtl's theory. This OCT consists of three bladed single rotor. Each blade is going to be divided to 25 sections in order to implement the BEM (Blade Element Momentum) algorithm. Each cross-section is a two-dimensional airfoil profile, each a member of the original FX77-W foil family. We use JavaFoil which is a new implementation of the old CalcFoil program that was written using C language. The hydrofoils selection is based on preliminary works on research turbine that have been done at Southeastern National Marine Renewable Energy Center (SNMREC). Numerical and experimental investigation have been conducted in several designs. Wenlong Tian et al. performed three-dimensional transient simulation to study the hydrodynamic performance of an OCT with a 3 m diameter three-bladed. In this study 3D transient RANS CFD simulations were performed to study the performance, including power, thrust and wake characteristics, of a 3 m diameter turbine designed by SNMREC. Simulations were performed to evaluate the impact of yaw angle and turbulence intensity on the performance of the turbine. In this paper the CFD model of the horizontal hydrokinetic turbine is described in detail, including the size and generation method of the mesh, the step size and the solution settings.[8]. Michael Borghi et al. described an ocean current turbine rotor design methodology that could be fitted to a small-scale experimental research turbine [9]. James VanZwetien et al. developed a numeric simulation for predicting OCT performance. This paper details the development of a numeric simulation for estimating the performance of ocean current turbines that are moored using a single mooring line. This modeling method calculates the drag on all the system's major components and uses an unsteady BEM rotor model to estimate the forces on the rotor for dynamic inflow conditions and offaxial flows. Wave and current models are included in this simulation so that performance prediction can be made in the expected operating environment. Their model predicted that the OCT will have a maximum rotor power coefficient of 0.45 which is in a good agreement with our current study [6]. Also, Matt Edmunds et al. described a new computational method for the accurate modelling of the interaction of renewable energy turbines with a fluid. As these devices will provide increasing amounts of global energy in future, this is an important topic. A balanced judgement should be made of the required length scales and ac- curacy compared to computational cost. The method sits between highly detailed blade resolved models and larger scale oceano-graphic and atmospheric models. It is important to not only be able to predict turbine performance at peak operating conditions, but throughout the entire TSR range. The use of analytical methods to successfully and accurately predict the distribution of lift towards the tip of finite wing, i.e. accurately predicting 'roll off' losses for a given foil geometry and chord distribution, are demonstrated to produce excellent results for the accurate prediction of power and thrust. Allowing for the variation of foil section shape within the model adds to the refinements including the distribution of forces along the foils. This helps produce better characteristics closer to the rotor hub, and also improved prediction in the stall region of the TSR range. [16] In addition, Jams VanZweiten et al. presents an overview of a design process used to create a preliminary hydrodynamic design of a stall regulated rotor blade for an experimental ocean current turbine designed to operate in the Florida Current off of Southeast Florida. This process utilized 13 months of continuous current measurements to create a flow probability function that was used in the design process. This design process used 39 different hydrofoil shapes designed for wind turbines to create 15 optimized rotor designs. The optimized rotor design created from FX-77-W airfoils was predicted to produce the largest mean shaft power. The geometry and predicted performance of this rotor was also presented. Finally, a sensitivity analysis was presented to quantify how varying the operating RPM, rated power, and the number or rotor blade changes the predicted average power production for an optimized rotor blade. Also, their optimized rotor blade design was predicted to produce a mean shaft power of 7.153 kW when operating at 40 RPM [10]. This paper enhances numerical and experimental results presented in Ref. [6,8,9,10,16] in order to evaluate and characterize the performance of the OCT. The study is performed using an adjusted BEM algorithm to improve power performance specifications. Section 2 describes the method including the actuator disc concept, blade element momentum theory, Prandtl's approximation for tip-loss factor, determination of the torque, thrust and power. Section 3 addresses the geometric properties of the blades, hydrodynamic coefficients of each cross-section of the blades, determination of axial and tangential induction factors, determination of torque, thrust and power. Finally, a comparison for the validation purpose and maximum power based on the current speed is presented. This preliminary investigation is required to design and develop a small-scale research turbine to conduct a towing tank experiment.

2. MATERIALS AND METHODS

2.1 The Actuator Disc Concept

For simplicity, let's start an analysis of the aerodynamic behavior of the OCT without considering any specific turbine design characteristic by replacing an actuator disc instead of the OCT in the sea-water to extract kinetic energy. Suppose that, as shown in the figure 1, the cross-sectional area of the upstream is smaller than the cross-sectional area of the actuator disc and the downstream has the largest cross-sectional area in the channel. The mass of the water which passes through the channel in the given cross section of the channel is equal to ρAU . By considering the law of the conservation of mass:

$$\rho A_{\infty} U_{\infty} = \rho A_d U_d = \rho A_w U_w \tag{1}$$

Which the subscripts ∞ , d and w denote the condition of the upstream (current speed), actuator disc and downstream. Due to the fact that the actuator disc induces some variation in the current velocity by an axial induction factor a, then

$$U_d = U_{\infty}(1 - a) \tag{2}$$

Also, by considering tangential velocity in addition to the axial velocity, we need to take the tangential flow induction factor a' into account. The tangential velocity in the upstream is zero, very close to the downstream of the actuator disc is $2\Omega ra'$ and also the tangential velocity of the wake is $\Omega ra'$.

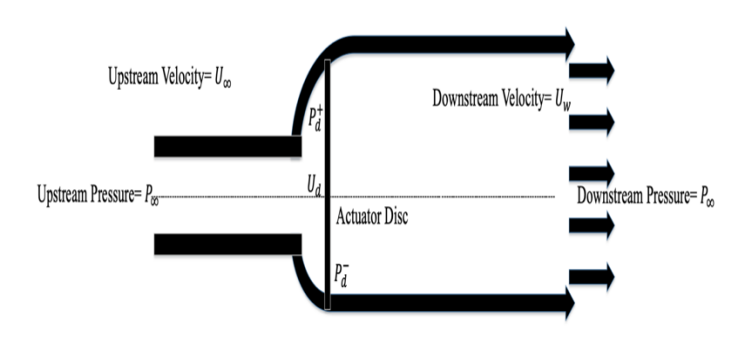


FIGURE 1: An Energy Extracting Actuator Disc and Stream-tube

2.2 Blade Element Momentum Theory

Blade Element momentum theory takes advantage of both Blade Element Theory and Momentum Theory. After brief analysis of the actuator disc, lets replace it with an actual 3-blade ocean current turbine which was designed by Florida Atlantic University research group [2]. As figure 2 (The airfoil was created by COMSOL Multiphysics.) indicates, the net tangential velocity of by the blade element theory is $\Omega r(1 + a')$, then the resultant velocity is defined as

$$W = \sqrt{U_{\infty}^2 (1 - a)^2 + \Omega^2 r^2 (1 + a')^2}$$
 (3)

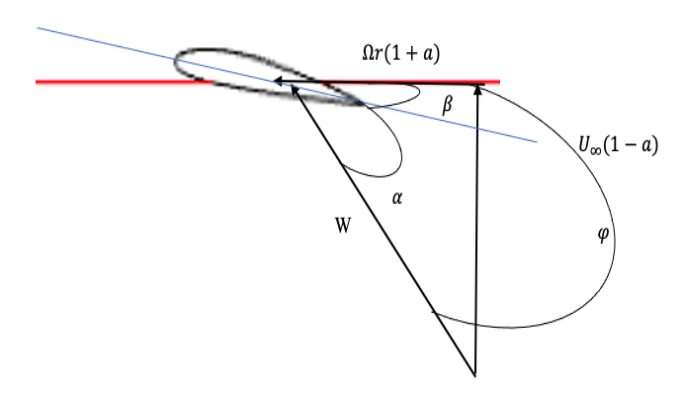


FIGURE 2: Blade Element Momentum Velocities

Given the information of the variation of the aerodynamic lift (C_l) and drag (C_d) coefficients in respect to the angle of attack for each cross sections of the blades, leads to the axial and tangential induction factors. By applying the laws of conservation of momentum and energy, as shown in the figure 2, for an individual OCT with N blades and with various chord lengths and pitch angles for 25 different cross sections,

$$\sin \varphi = \frac{U_{\infty}(1-a)}{W} \tag{4}$$

and

$$\cos \varphi = \frac{\Omega r(1+a')}{W} \tag{5}$$

Where $\varphi = \alpha + \beta$. Due to the definitions of the aerodynamic forces for each cross section. by looking into figure 3, the cross-sectional lift and drag forces are defined as,

$$\delta L = \frac{1}{2} \rho W^2 c C_l \delta r \tag{6}$$

$$\delta D = \frac{1}{2} \rho W^2 c C_c \delta r \tag{7}$$

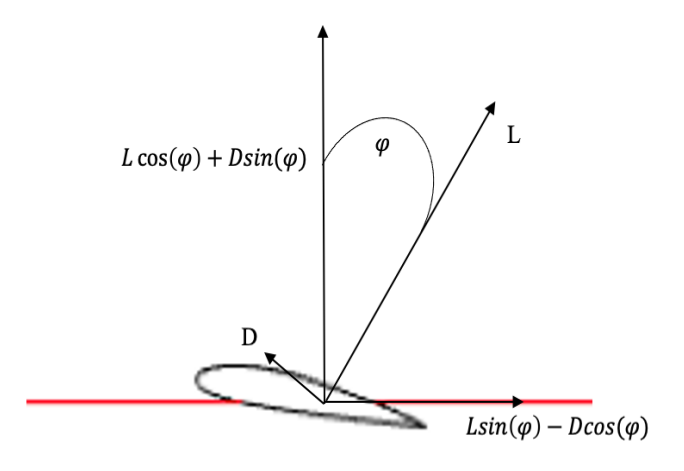


FIGURE 3: Blade Element Momentum Forces

Source: Burton, Tony. Wind Energy Handbook. Wiley, 2011.

So,

$$\delta L \cos \varphi + \delta D \sin \varphi = \frac{1}{2} N c \rho W^2 (C_l \cos \varphi + C_d \sin \varphi) \delta r$$
 (8)

It is convenient to use:

$$\mu = \frac{r}{R}$$
 (9)

$$C_x = C_l \cos \varphi + C_d \sin \varphi$$
 (10)

$$C_y = C_l \sin \varphi - C_d \cos \varphi$$
 (11)

Due to the nonlinearity of the system to obtain axial and tangential induction factors using two-dimensional hydrofoil characteristics, an iterative procedure is needed, the following equations are used:

(11)

$$\frac{a}{1-a} = \frac{\sigma_r}{4\sin\varphi^2} \left[C_x - \frac{\sigma_r}{4\sin\varphi^2} C_y^2 \right]$$
 (12)

$$\frac{a'}{1+a'} = \frac{\sigma_r}{4\sin\varphi\cos\varphi} \tag{13}$$

Where σ_r is chord solidity defined as the total blade chord length at a given radius divided by the circumferential length at that radius. [1]

$$\sigma_r = \frac{Nc}{2\pi r} = \frac{Nc}{2\pi \mu R} \tag{14}$$

Note that the BEM theory is only valid if the blades have uniform circulations.

Prandtl's Approximation for tip-loss factor 2.3

A reduced power is due to a reduced torque and this effect is known as tip loss, when it occurs only at the tip of the blades by reducing the lift force and generating torque. According to the Ludwig Prandtl's tip loss factor we have:

$$F = \frac{2}{\pi} cos^{-1} (e^{-f}) \tag{15}$$

where

$$f = \frac{N(R - r)}{2r\sin\emptyset} \tag{16}$$

And generally,

$$\frac{r}{R} \le 0.6$$
: $F \approx 1 \& \frac{r}{R} > 0.6$: $F < 1$ (17)

By including the tip-loss factor into the calculations, new equations will be obtained to calculate induction factors due to their iterative solutions.

$$a = \frac{1}{\frac{4\operatorname{Fsin}\varphi^2}{\sigma_r C_r} + 1} \tag{18}$$

$$a' = \frac{1}{\frac{4F\sin\varphi\cos\varphi}{\sigma_{\nu}C_{\nu}} - 1}$$
 (19)

2.4 Determination of the Torque, Thrust and

Using the designed rotor at its design rotational velocity of 50 RPM, the predicted shaft power, thrust, and torque can be derived from the momentum theory:

$$\delta Q = 4\pi \rho U_{\infty} a' (1 - a) \Omega r^3 \delta r \qquad (20)$$

$$\delta T = 4\pi \rho U_{\infty}^2 a (1 - a) r \delta r \tag{21}$$

$$\delta P = \Omega \delta Q = 4\pi \rho U_{\infty} a' (1 - a) \Omega^2 r^3 \delta r \qquad (22)$$

The in-house created BEM code to compute the axial and tangential induction factors iteratively and calculate the sectional forces for our individual OCT follows the flow chart that briefly illustrated in figure 4.

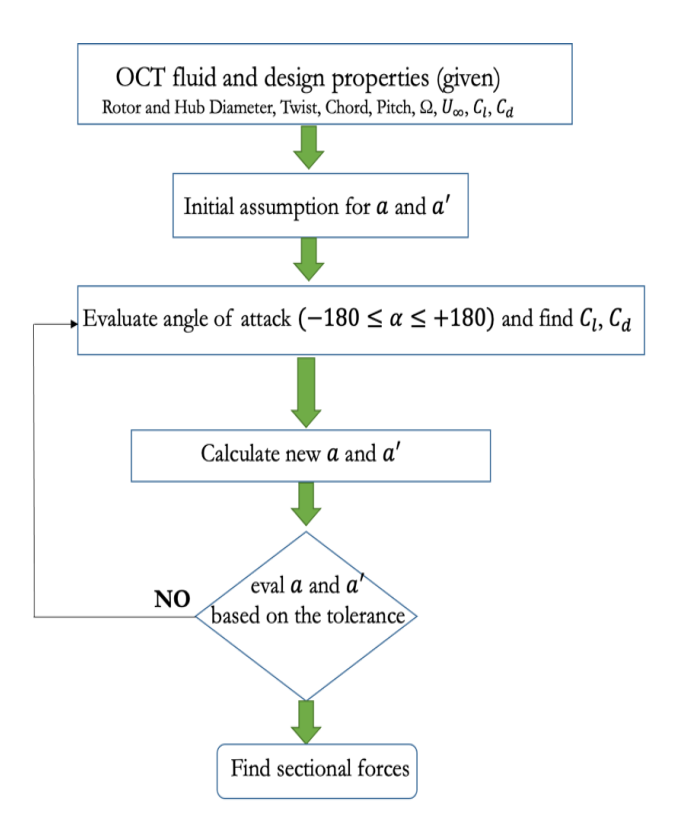


FIGURE 4. BEM theory Flow chart

3. RESULTS AND DISCUSSION

3.1 Geometric Properties of the Blades [2]

Figure 5 presents the shapes of 25 different hydrofoils that located from head to tip of each blade based on the given geometric properties for a rotor blade optimized to create the maximum amount of power from the Florida Current using a stall regulated rotor operated at 50 RPM. This rotor is designed to be used on a 20 kW experimental ocean current turbine and the stall regulated rotor blade is being designed to produce a maximum of approximately 20 kW of shaft power when operating at its design rotational velocity. [3]

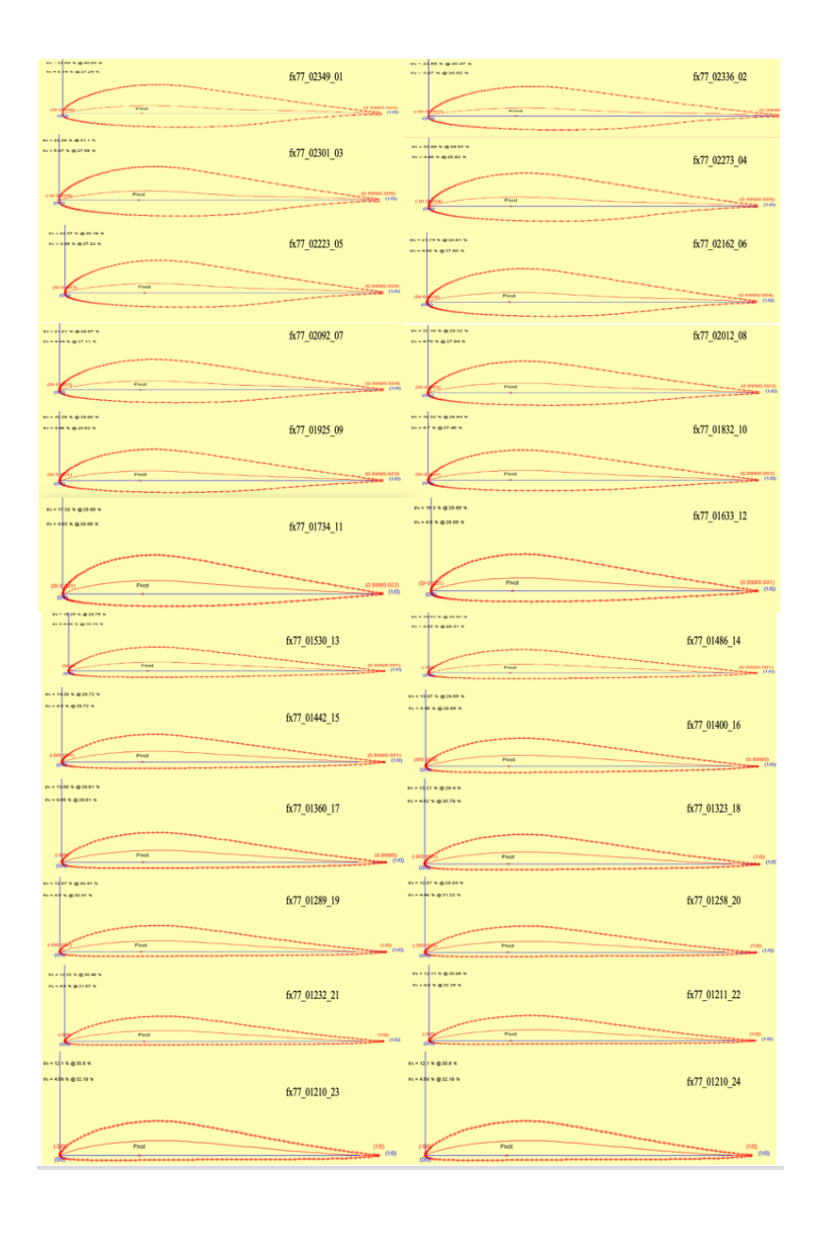


FIGURE 5: Geometric Shapes of the Cross-Sectional Hydrofoils

The percent thicknesses range from 12.1-23.49 and therefore the geometric shapes of these airfoils come from the original FX77W121 airfoil shape and from interpolating between the FX77W121, FX77W153, and FX77W258 airfoil shapes, as the last three digits of this airfoil family approximate the thickness ratio times 1000 (FX77153 => 15.3 % thickness ratio). Of the 25 different airfoil shapes specified for the optimal rotor, there are 23 unique shapes. [4]These 25 airfoil coordinate files are given in the 25 files called fx77 02349 01, fx77 02336 02, fx77 02301_03, fx77 02273 04, fx77 02223 05, fx77 02162 06. fx77 02092 07. fx77 02012 08, fx77 01925 09, fx77 01832 10, fx77 01734 11, fx77 01633 12, fx77 01530 13, fx77 01486 14, fx77 01442 15, fx77 01400 16, fx77 01360 17,

fx77_01323_18, fx77_01289_19, fx77_01258_20, fx77_01232_21, fx77_01211_22, fx77_01210_23, fx77_01210_24, and fx77_01210_25, which ideally should accompany this report but space restrictions do not permit. Figure 6 shows how the chord length of each rotor blade is changing by increasing $\frac{r}{R}$.

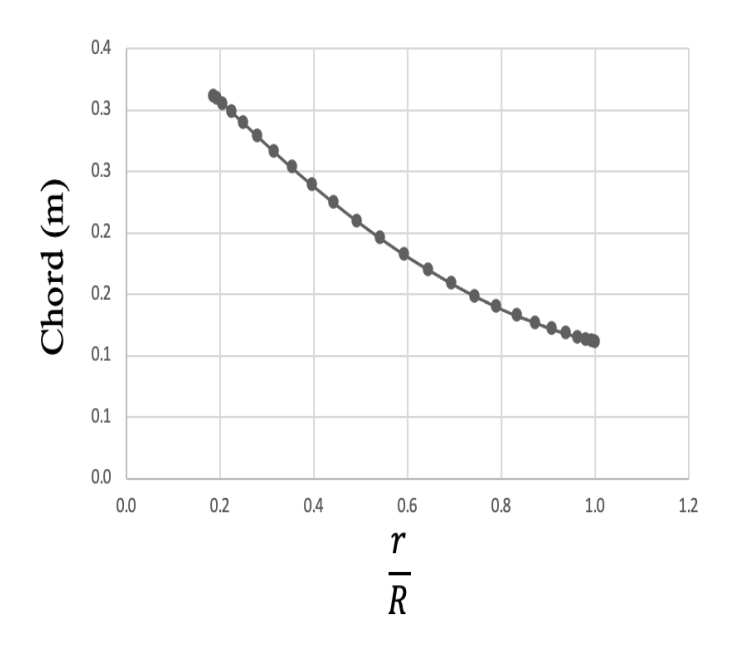


FIGURE 6: Chord Length vs. $\frac{r}{R}$

Figure 7 indicates the data flow of rotor blade pitch angle which is varying between 0-27°.

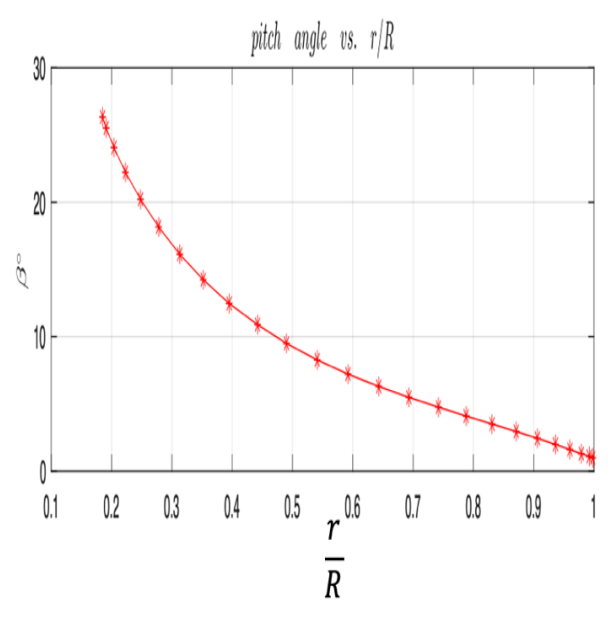


FIGURE 7: Pitch angle Length vs. $\frac{r}{R}$

3.2 Hydrodynamic Coefficients of Each Cross-Section of the Blades [11]

Based on the geometric properties of each blade cross-

section, lift and drag coefficients along the spanwise of the rotor blades from tabulated airfoil data are calculated by Javafoil. Javafoil is a web-based program that uses C language to run several traditional airfoil analyses. This program calculates the moment, lift, and drag characteristics of the airfoil very fast and accurate. The first step is to calculate the distribution of the velocity on the surface of the foils by considering the potential flow analysis module that follows a higher order panel method. By using Bernoulli's equation, the velocity and pressure fields is obtained. Then by the integration of the local pressure field along the airfoil surface, the lift coefficients are calculated. Then, by considering the stagnation point as the first point, the program

starts to calculate the behavior of the flow in boundary layers,

along the upper and lower surfaces of the foil. The drag coefficients of the airfoil are calculated by solving a set of

differential equations for any angle of attack.[11]

In our research, the lift and drag coefficient are calculated with respect to the angle of attack between $(-180 \le \alpha \le 180)$ for further use in the BEM code to calculate the induction factors. In this analysis, the Reynolds numbers is fixed as 16×10^5 . Figure 8 indicates how lift coefficients are changing with respect to the angle of attack for each hydrofoil. The range of the lift coefficients is $(0.214 \le c_l \le 2.212)$ when $(0 \le \alpha \le 20)$. Figure 9 shows the behavior of the drag coefficient which is confined to the range $(0.00983 \le c_d \le 0.291)$ for the angle of attack $(0 \le \alpha \le 20)$.

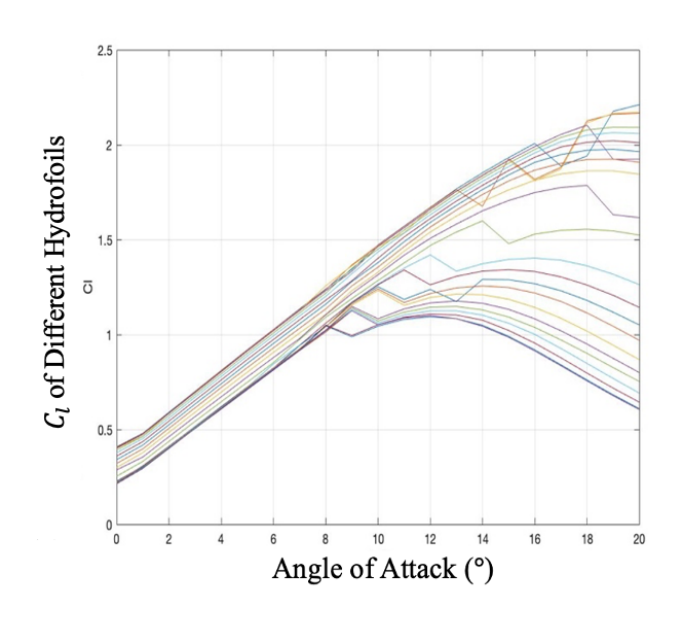


FIGURE 8: Lift Coefficient vs. Angle of Attack for all the 25 Cross-Sections

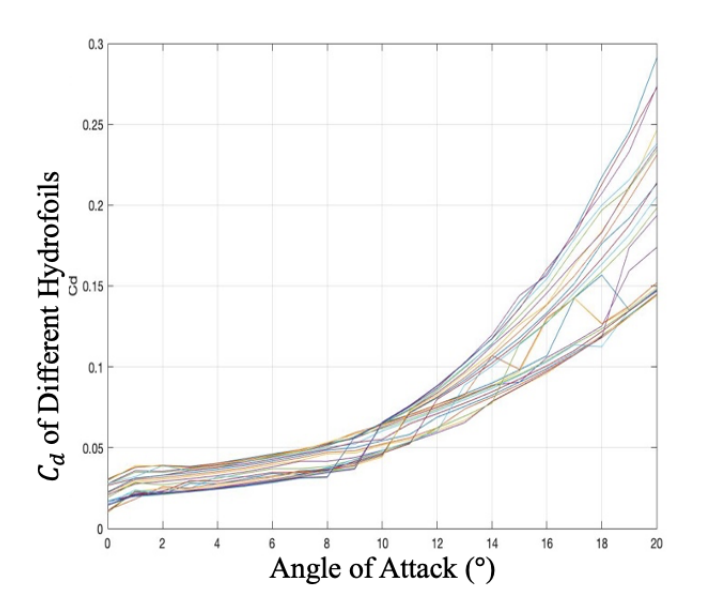


FIGURE 9: Drag Coefficient vs. Angle of Attack for all the 25 Cross-Sections

3.3 Determination of Axial and Tangential Induction Factors

Figure 10 shows the inflow angle which is the addition of the angle of attack and the pitch angle between $(0 \le \varphi \le 32)$ with respect to the parameter μ . Figure 11 shows the axial and tangential induction factors of the rotor blade which are calculated iteratively by the BEM code. These two factors are necessary to analyze the performance of the turbine. The behavior of the axial induction factor $(0.1769 \le a < 1)$ is increasing with respect to μ , but, the behavior of the tangential induction factor is decreasing with respect to μ in the range of $(0 < a' \le 0.0722)$. Results of the axial and tangential induction factors show good agreement with the results of the research provided by the University of Notre Dame that shown in Figure 12. [5]

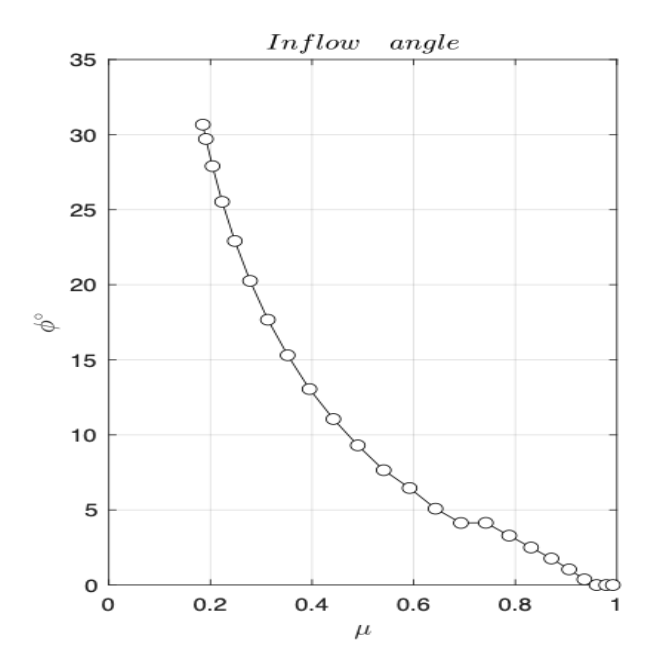


FIGURE 10: Inflow Angle vs. $\frac{r}{R}$

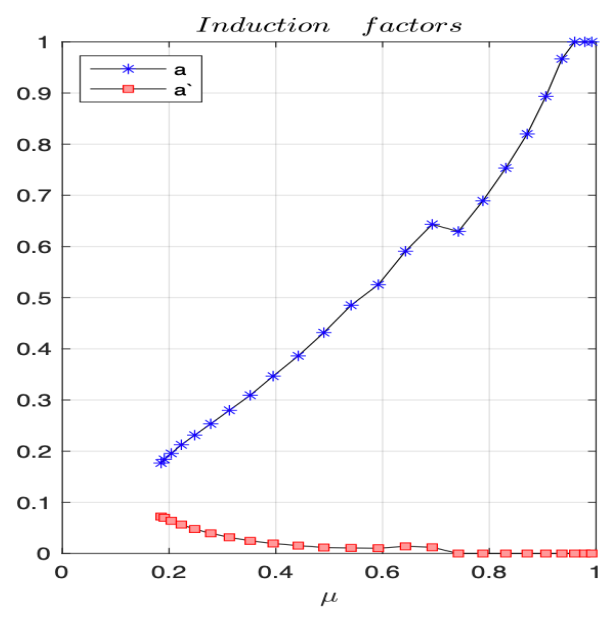


FIGURE 11: Axial and Tangential Induction Factors vs. $\frac{r}{p}$

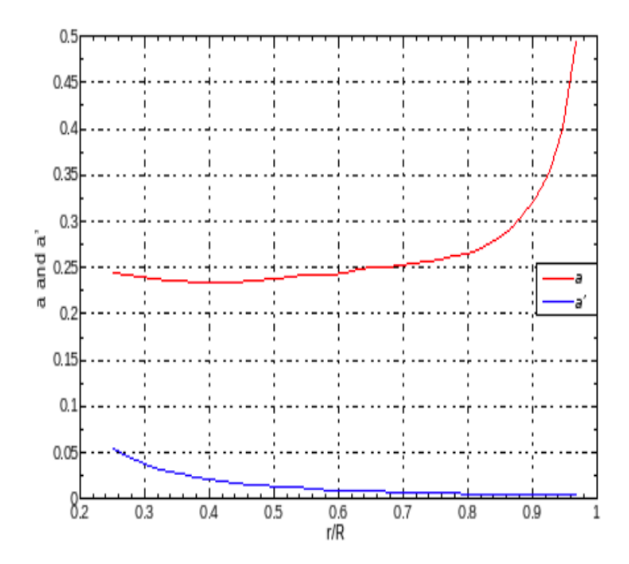


FIGURE 12: Axial and Tangential Induction Factors vs. $\frac{r}{R}$ From the University of Notre Dame Data, Source of the figure [5]

3.4 Determination of Torque, Thrust and Power

The spanwise distribution of the differential thrust, torque, and power are indicated in figures 13, 14, and 15. These results show reasonable agreement with the results of [5]. In all the below-mentioned figures, the peaks of the thrust, torque, and power are located around $\mu \approx 0.7$.

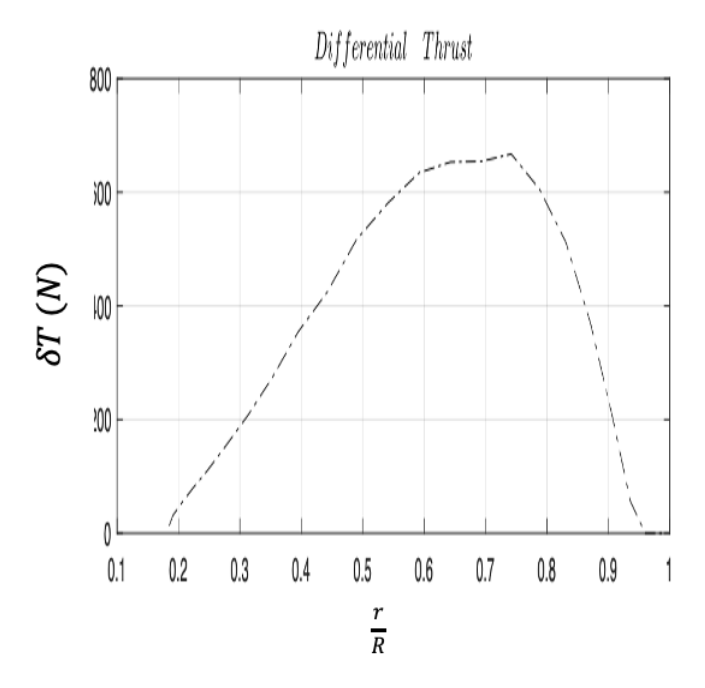


FIGURE 13: Differential Thrust vs. $\frac{r}{R}$

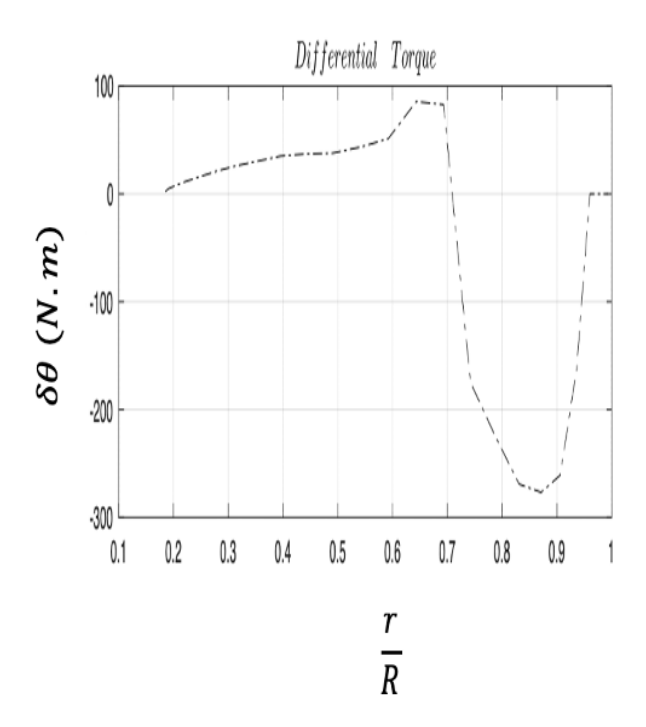


FIGURE 14: Differential Torque vs. $\frac{r}{R}$

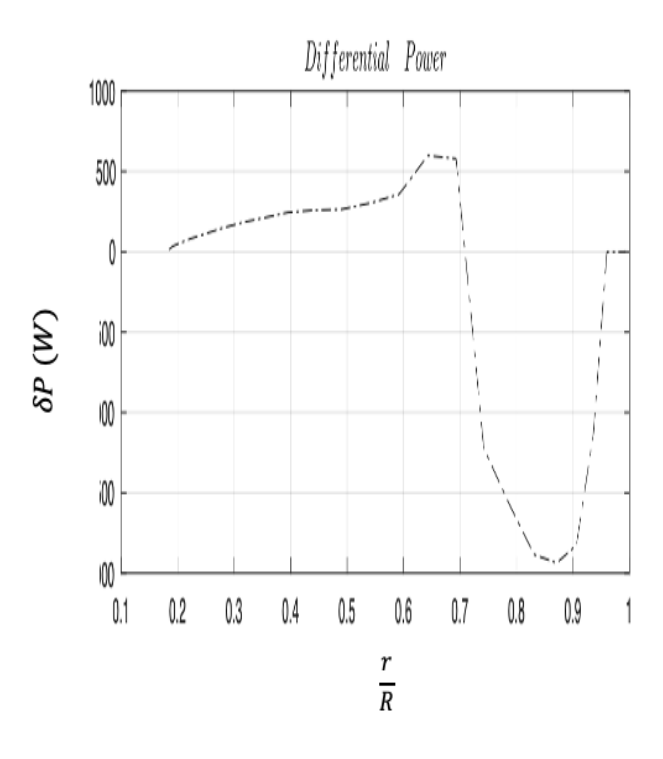


FIGURE 15: Differential Power vs. $\frac{r}{R}$

3.5 Maximum Power Based on the Current Speed

According to our BEM code, the maximum rotor power coefficient for the turbine is $C_p = 0.4390$, which is close to the predicted maximum rotor power coefficient $C_p = 0.45$ done by the James H. VanZwieten, Jr., Nicolas Vanrietvelde, and Basil L. Hacker, Student Member, IEEE, Numerical Simulation of an Experimental Ocean Current Turbine [6]. Ocean current measurements were taken off Southeast Florida (Lat: 26°04.3′N. Lon: 79°50.5′W) over a 13-month period from February 2009eMarch 2010 [7,8]. These measurements show that the mean current speed at a depth of 25 m was 1.6 m/s, with a range between 0.4 and 2.5 m/s. [7,8]. Figure 15 shows the maximum power curve of the ocean current turbine for different current velocities as described above. The maximum power is considered as 20kw based on the [3,6,8]. This data will be compared with experimental data in our following research that is conducting in the University of New Orleans towing tank with the experimental scaled ocean current turbine. As it is shown in the figures 15 and 16, the power curves follow the same trend in respect to the flow velocity. In the future, behavior of the thrust and power distribution will be investigated as indicated in the figure 16.

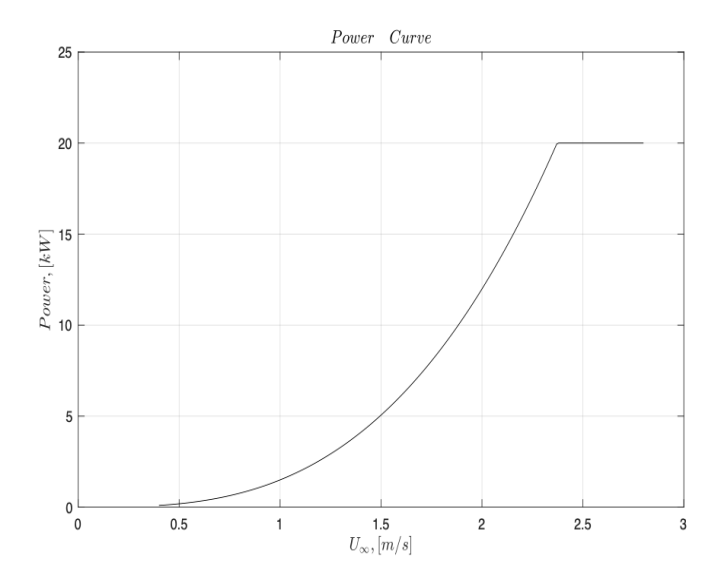


FIGURE 15: Maximum Power Curve vs. Current Velocity

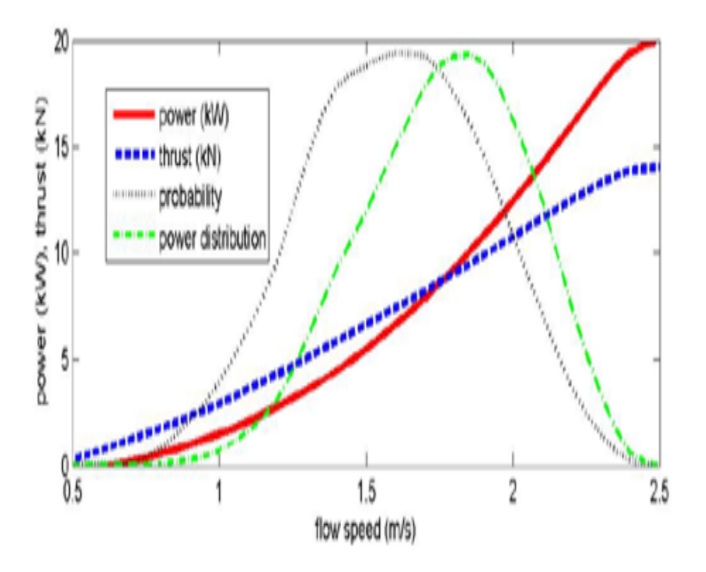


FIGURE 16: Maximum Power Curve vs. Current Velocity based on the research in [10], Source of the figure:[10]

4. CONCLUSION

In this paper, we have implemented a Blade Element Momentum theory code based on the provided experimental scale ocean current turbine geometry to analyze the performance of the turbine by considering hydrodynamic forces, axial and tangential induction factors, the spanwise contribution of differential torque thrust and power and hydrodynamic coefficients from the JavaFoil based on the Panel method. The most important reason that we developed BEM code are as follows: First of all, this theory directly combines blade element theory and momentum theory, and consider their requirements in one theory, Also, getting the axial and tangential induction factors from the BEM theory is completely straight forward in compare to other theories. In addition, we will be using this BEM code to predict our new current research required information such as different forces and induction factors to compared new experimental power, torque and thrust with the developed BEM code.

ACKNOWLEDGEMENTS

The authors would like to thank the National Science Foundation (NSF) and specifically the Energy, Power, Control and Networks (EPCN) program for their valuable ongoing support in this research within the framework of grant ECCS-1809182 'Collaborative Research: Design and Control of Networked Offshore Hydrokinetic Power-Plants with Energy Storage'.

REFERENCES

- [1] Burton, Tony, Wind Energy Handbook, Wiley, 2011
- [2] James H. VanZwieten, Report, SNMREC Rotor Blade Design and Predicted Performance.
- [3] James H. VanZwieten, Parakram Pyakurel, Tri Ngo, Cornel Sultan, Nikolaos I. Xiros, An assessment of using variable blade pitch for moored ocean current turbine flight control, International Journal Of Marine Energy 16-26, 2016.
- [4] C.M. Oster "Optimization of a Hydrodynamic Rotor Blade", Summer Internship Final Report, COET (SNMREC), August, 2010
- [5] Aerodynamic Performance, *University of Notre Dame, AME,* 40530.
- [6] James H. VanZwieten, Jr., Nicolas Vanrietvelde, and Basil L. Hacker, *Student Member, IEEE, Numerical Simulation of an Experimental Ocean Current Turbine.*
- [7] Duerr AES, Dhanak MR. *Hydrodynamic Power Resource Assessment of the Florida Current, In: MTS/IEEE ocean conference 2010. Seattle; September* 20-23, 2010.
- [8] Wenlong Tian, James H. VanZwieten, Parakram Pyakurel, Yanjun Li, Influences of yaw angle and turbulence intensity on the performance of a 20 kW in-stream hydrokinetic turbine, Energy Journal, Available online 3 June 2016.
- [9] Michael Borghi, Fumbi Kolawole, Sathya Gangadharan, Willoam Engblom, James H. VanZwieten, Gabriel Alsenas, William Baxley, Shirely Ravenna, *Design, Fabrication and Installation of a Hydrodynamic Rotor for a Small-Scale Experimental Ocean Current Turbine*.
- [10] James H. VanZwieten, Carey Oster, Alana Duerr, Design ana Analysis of a Rotor Blade Optimized for Extracting Energy from the Florida Current.

- [11] JavaFoil User's Guide, Martin Hepperle, 22-Dec-2017.
- [12] S. Rouhi, N. Xiros, S. Sadeqi, J. Ioup, J. VanZwieten, C. Sultan, "CFD Validation of the Thermodynamic Model of a Compressed Gaseous Hydrogen Storage Tank". American Society of Thermal and Fluids Engineers.) TFEC-2020-36525, 2021.
- [13] S. Sadeqi, N. Xiros, S. Rouhi, J. Ioup, J. VanZwieten, C. Sultan, "Wavelet Transform Analysis Applied to Incompressible Flow Field About a Solid Cylinder". American Society of Thermal and Fluids Engineers, TFEC-2020-36526, 2021.
- [14] S. Rouhi, S. Sadeqi, N. Xiros, J. Ioup, "CFD Analysis of Filling Process for a Hydrogen Energy Storage System". American Society of Thermal and Fluids Engineers. TFEC-2020-32066, 2020.
- [15] S. Yoshida, F. Miura, T. Sasaki, S. Rouhi, "Optical Analysis of Residual Stress with Minimum Invasion". The Society for Experimental Mechanic (SEM) annual/volume 8/paper 141. (2017)
- [16] Matt Edmunds, Alison J. Williams, Ian Masters Arindam Banerjee, James H. VanZwieten, A spatially nonlinear generalised actuator disk model for the simulation of horizontal axis wind and tidal turbines.